AER/AGS Special Report 131

Alberta Energy Regulator

Analysis of WorldView-3 Satellite Imagery for the Wylie Lake Area, Northeastern Alberta

AGS
ALBERTA GEOLOGICAL SURVEY

AER/AGS Special Report 131

Analysis of WorldView-3 Satellite Imagery for the Wylie Lake Area, Northeastern Alberta

B. Rivard and J. Feng

Department of Earth and Atmospheric Sciences, University of Alberta

June 2026

ISBN 978-1-4601-5746-6

Rivard, B. and Feng, J. (2026): Analysis of WorldView-3 satellite imagery for the Wylie Lake area, northeastern Alberta; Alberta Energy Regulator / Alberta Geological Survey, AER/AGS Special Report 131, 24 p.

Publications in this series have undergone only limited review and are released essentially as submitted by the author.

Authors' address:
B. Rivard and J. Feng
Department of Earth and Atmospheric Sciences
University of Alberta
1-26 Earth Sciences Building
Edmonton, AB T6G 2E3
Canada

Tel: 780.953.7110
Email: bentrivard9@gmail.com

Published June 2026 by:
Alberta Energy Regulator
Alberta Geological Survey
Suite 205
4999 – 98 Avenue NW
Edmonton, AB T6B 2X3
Canada

Tel: 780.638.4491
Email: AGS-Info@aer.ca
Website: ags.aer.ca

Contents

Figures

Foreword

As part of the Alberta Minerals Strategy and Action Plan, the Alberta Energy Regulator / Alberta Geological Survey acquired Maxar WorldView-3 satellite imagery over the Canadian Shield in northeastern Alberta. This acquisition was undertaken to support the detection and mapping of metallic mineral occurrences, where documented deposits of gold, base metals, uranium, and rare-earth elements are found in narrow belts associated with major shear zones.

In November 2024, Professor Emeritus Benoit Rivard and Dr. Jilu Feng were contracted to conduct a detailed analysis of WorldView-3 satellite imagery for the Wylie Lake district, building on previous work in the Leland Lakes and Andrew Lake areas. This study sought to identify mineralization potential by detecting exposed rock outcrops, delineating lithological units, and mapping mineral alteration features within the Alberta portion of the Canadian Shield.

This report presents key findings that expand the understanding of lithological and mineral alteration patterns within the Wylie Lake area. The analysis identified zones with significant internal variability within primary rock units, particularly in the granite gneiss and granitoid complexes. These zones revealed elevated concentrations of minerals such as white mica, biotite, and chlorite. Through the use of a ‘White mica index’ and other spectral indices, previously unidentified areas rich in hydroxyl-bearing minerals were detected. These minerals are present in biotite schists, amphibolite, and metasedimentary layers. This highlights mineralogical diversity that points to potential subunits within the primary mapped units.

Preprocessing involved masking non-rock features such as vegetation, water, burns, and shadows to refine the detection of rock outcrops. Key spectral indices were applied to analyze iron- and hydroxyl-bearing minerals, facilitating the distinction between mafic and felsic lithologies. Spectral angle mapping (SAM) was used with both image-derived and field-collected endmembers, yielding detailed spectral maps that highlighted zones of potential mineralization and specific lithological contrasts.

This report’s findings underscore the potential of utilizing WorldView-3 satellite imagery for accurately mapping complex lithological features and identifying zones of mineralization, particularly in areas with extensive vegetation cover. Field validation is recommended to confirm remote sensing interpretations and to refine exploration strategies in northeastern Alberta.

Aside from the cover, copyright information, and this page, the report is published as received from the vendor (with minor editing).

This work was completed under the Mineral Grant provided by the Government of Alberta dated June 22, 2021.

1 Introduction

This report summarizes the analysis of WorldView-3 imagery over the Wylie Lake district in Alberta (Figure 1) as part of AER Service Agreement 24SA-SR008. As in two prior studies for Leland Lake (Rivard 2023) and Andrew Lake (Rivard and Feng 2024), the area encompasses extensive vegetation cover and the analysis aimed to isolate exposed outcrop, delineate lithologic units and detect and map potential mineral alteration. The limited spectral dimensionality of WorldView-3 data implied a focus on the detection of iron oxides and OH- bearing minerals (e.g. white mica and biotite, chlorite, amphibole as a group). This work is conducted as part of an initiative to detect potential metallic mineral occurrences in the Alberta shield where known occurrences of gold, base metals, uranium, and rare-earth elements have been documented (Godfrey 1980, Langenberg and Eccles 1996). These mineral occurrences are associated with alteration on the surface such as weathered sulphide horizons, schists, and pegmatites or, in the case of widespread radioactivity, abundant yellow stains. The satellite data analysis follows the process established for the analysis of WorldView-3 imagery for the Leland Lake area in 2022-2023 as part of the AER/AGS Special Report 116.

Figure 1. Google map view with white polygon located in the northeastern Alberta and defining the area of interest encompassed by the WorldView-3 satellite data.

2 Satellite Data

Two lines of WorldView-3 satellite data acquired on October 16, 2021, and June 8, 2022, encompass the area of interest in northeastern Alberta (Figure 1). Each line was delivered as two datasets. The visible near infrared data (VNIR) has 8 spectral bands centered nominally at 427, 482, 547, 604, 660, 723, 824, and 914 nm with a spatial resolution of 1.24 m. The shortwave infrared data (SWIR) has 8 spectral bands centered nominally at 1209, 1572, 1661, 1730, 2164, 2202, 2259, and 2329 nm with a spatial resolution

of approximately 4 m. Preprocessing of the data conducted by the data provider included an atmospheric correction (ACOMP) with SCA correction applied to both datasets to minimize stripping, a standard orthorectification with nearest neighbour resampling, and an alignment correction (i.e. a boresight correction) for both dataset to enable their joint analysis. The data delivered is thus orthorectified imagery at surface reflectance and the SWIR data is resampled to 1.24 m to provide a 16-band spectrum per 1.24 m pixel. Figure 2 includes a "true color" mosaic (approx.1133 km^2) of the two lines encompassing the area of interest.

Despite the corrections listed above there remained a misalignment of VNIR and SWIR data noted on the borders of each line, as reported in the Andrew Lake study which uses the same data further north (Rivard and Feng 2024). Consequently, when the mosaic of the two lines was assembled for varying products, portions of each line encompassing misalignment were removed, and use of the June 2022 scene was maximized as it revealed more outcrop. This insured removal of alignment errors in the mosaic and derived products.

3 Methods

The methods are as described in Rivard (2023) and Rivard and Feng (2024) for the Leland Lake and Andrew Lake studies with minor adjustment to specific variables (e.g. mask thresholds). Several image processing methods were used, first to isolate pixels occupied by outcrop and generate an outcrop distribution map, and then to extract lithological information. The first set of methods relate to the generation of an outcrop map and involve masking all pixels not occupied by outcrop. Those include pixels affected by water, vegetation, and in shadow. The second category of methods includes the computation of spectral indices, the extraction and analysis of image spectral endmembers, and the analysis of reflectance spectra collected in the field all aiming to highlight lithological/alteration information.

3.1 Masking

Three masks (Equations 1-3) were designed for masking of vegetation, water, and shadows. A normalized vegetation index (Equation 1) was calculated for every pixel in the VNIR data to mask standing water (e.g., lakes, rivers), and vegetation. The Shadow index (Equation 2) (Shedlovska and Hnatushenko, 2019) minimizes the impact of shadows (including cloud shadows) and recent fire scars. The albedo mask (Equation 3) was also found to help delineate outcrops when dealing with two scenes with different solar illumination angles impacting shadows. For this index, focus is given to bands in the shortwave infrared where outcrops have highest reflectance, specifically from band 7 (830 nm) to band 17 (2330 nm). The value of 5000 is used to scale the results to 0-1.

Equation (1) NDVI index = (VNIR 7-VNIR 5) / (VNIR 7+VNIR 5)

Equation (2) Shadow index = (VNIR 8 – VNIR 2) / (VNIR 8 – VNIR 2) – VNIR 7

Equation (3) for Albedo

$$Albedo = \frac{1}{10.0} * \sum_{band=7}^{16} \frac{DN^{band}}{5000.0}$$

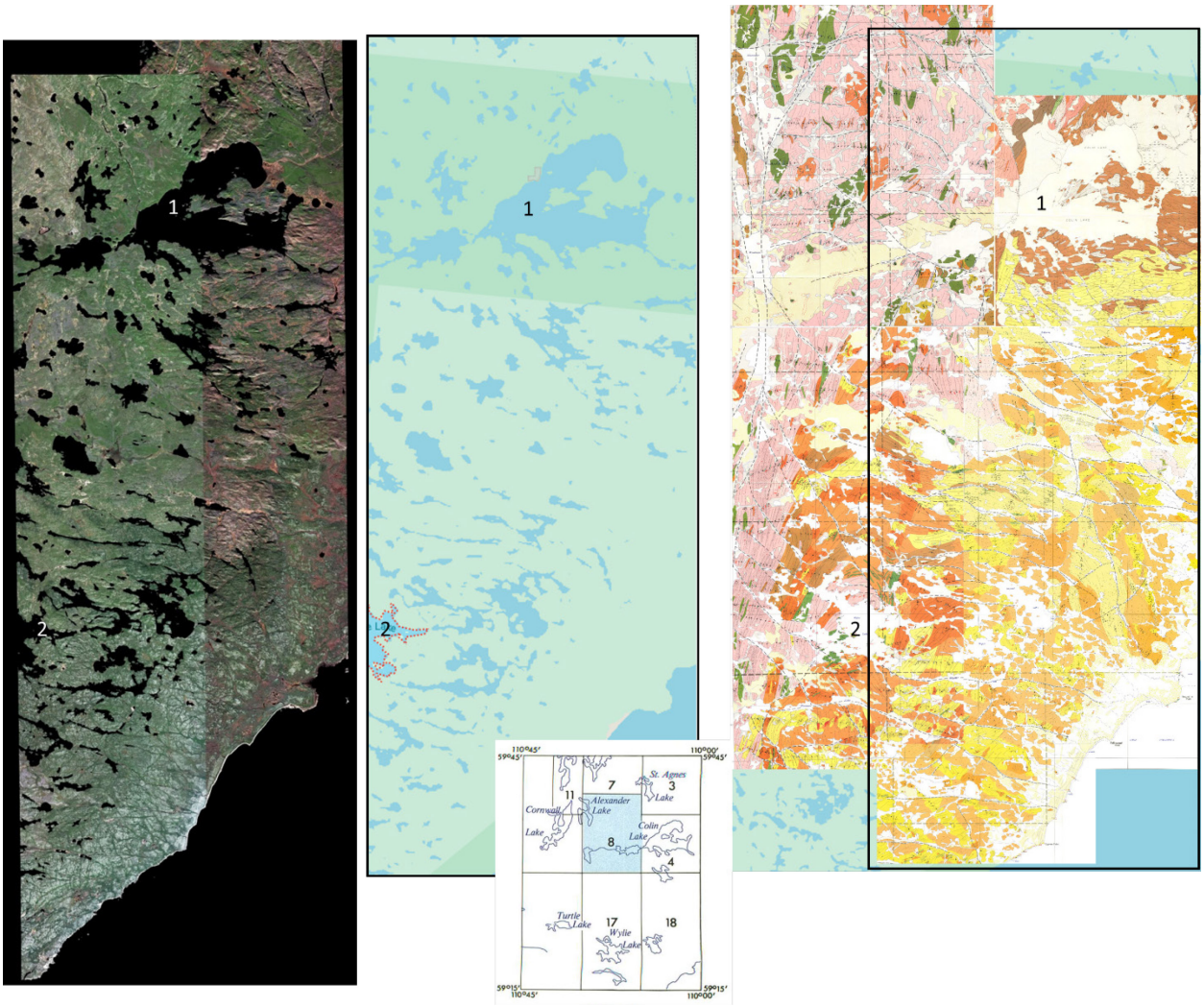

Figure 2. "True color" mosaic of the two WorldView-3 lines (left) and equivalent partial area encompassed by prior 1:31680 regional geologic mapping (right). The latter includes maps 4,8,17,18 and 19 of Godfrey (1980). Labels 1 and 2 refer to Colin Lake and Wylie Lake respectively.

3.2 Generation of an Outcrop Map

To derive the outcrop distribution map, shown on Figure 3, from which the lithological/alteration analysis could be conducted, the following thresholds were used in a first step to remove water, and shadows: pixels were retained if the NDVI was greater than 0.01 (water mask), the Shadow index was <0.5 and the Albedo was <0.02. In a second step to isolate outcrops from vegetation, the following thresholds were used: pixels were retained if NDVI <0.28 for the June scene and <0.35 for the October scene. In addition, pixels were retained if the Albedo >0.34 for the June scene and >0.45 for the October scene.

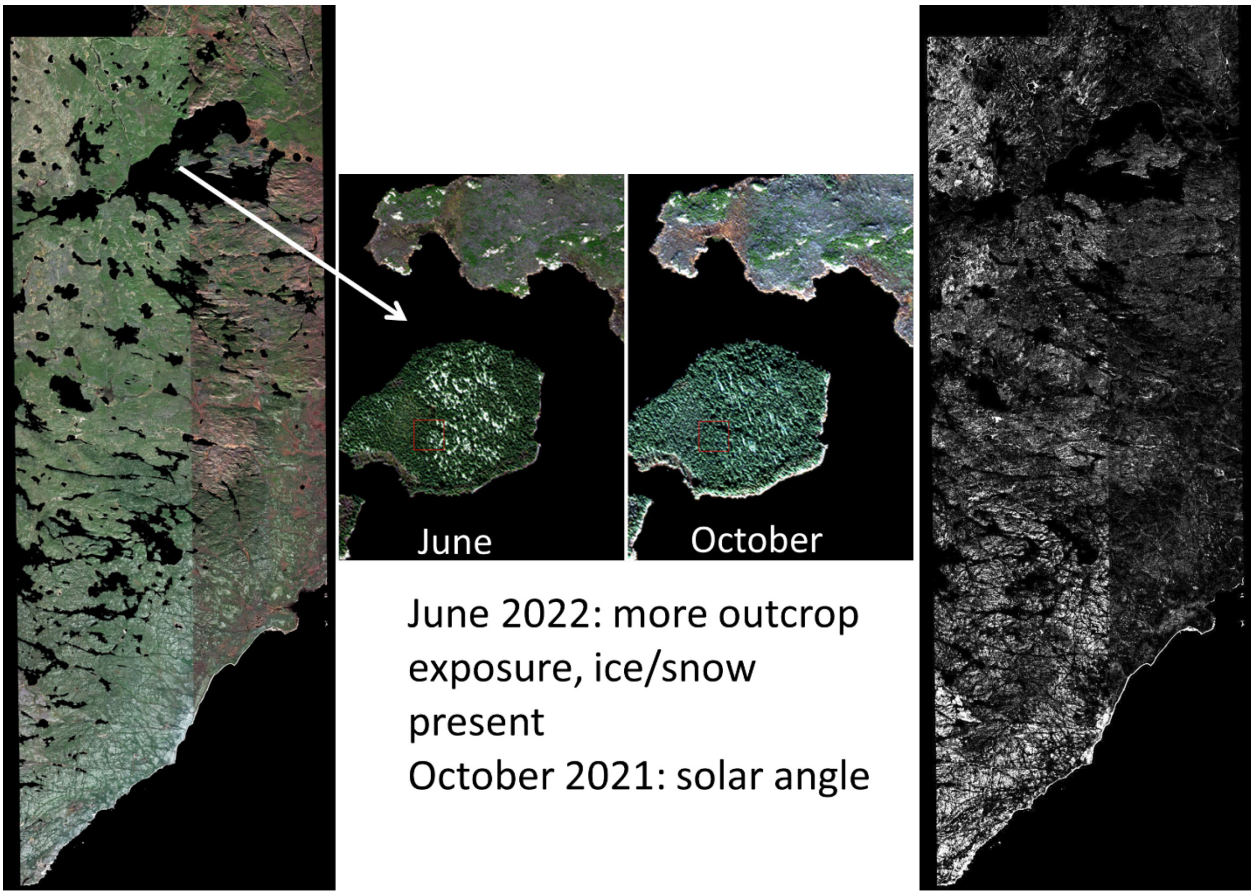

Figure 3. "True color" mosaic of the two WorldView-3 lines encompassing the area of interest (left). Disparities in the state of the vegetation are apparent between the June 2022 (left) and October 2021 (right) scenes. The resulting outcrop map is shown on the right.

3.3 Extraction of Lithological Information

3.3.1 Indices

As described in the AER/AGS Special Report 116 for the Leland Lake area, three indices were devised to capture mineralogical and thus lithological information related to the presence of hydroxyl (OH^-) and iron (Fe^{3+}) bearing minerals (e.g., white mica and iron oxides, Mars (2018)) seen in WorldView-3 image spectra (Figure 4).

The "White Mica index" is listed in Equation 4 and consists of a normalized ratio of two bands (SWIR5, SWIR6) at 2164 and 2202 nm respectively and thus capitalises on the white mica absorption feature located nominally at 2200 nm. Its intent is to inform on the relative abundance of white mica. The "Rock MF (Mafic Felsic)" index and the "Rock Fe (iron)" index are listed in Equation 5 and 6 respectively. The Rock Fe is designed specifically to measure the strength of the iron absorption nominally centered on band VNIR 7 located near 900 nm.

Equation (4) White Mica = (SWIR 5 - SWIR 6) / (SWIR 5 + SWIR 6)

Equation (5) Rock MF = (VNIR 3 + SWIR 3) / (VNIR 5 + VNIR 7)

Equation (6) Rock Fe = ((VNIR 6-VNIR 7) / (VNIR 6+VNIR 7)) + ((VNIR 8-VNIR 7) / (VNIR 8+VNIR 7))

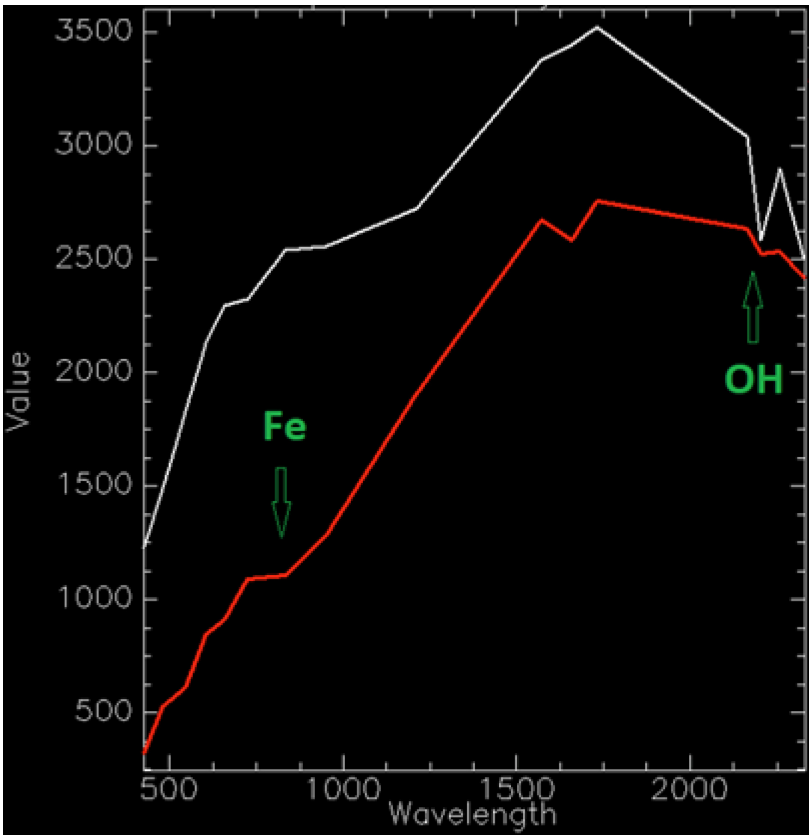

Figure 4. Example WorldView-3 spectra showcasing a strong iron (Fe) absorption near 900 nm (red spectrum) and a strong hydroxyl (OH^-) absorption near 2200 nm (white spectrum).

3.3.2 Use of Image Endmembers

The use of spectral endmembers is one approach to explore the data for lithologic information. Endmembers represent "purest" spectra of representative materials in the scene. Endmembers can be collected in the field or laboratory from known surfaces (outcrop or samples respectively) or extracted from imagery. The latter is commonly preferred for two reasons: 1) laboratory and field spectra may not capture all relevant surface components or may be inadequate representations (e.g., fresh rather than exposed weathered surfaces); and 2) image endmembers sample surfaces directly from the scene and are collected under the same viewing and illumination conditions as all spectra in the scene. Image endmembers are assumed to be relatively pure spectra, meaning that minimal mixing with other endmembers has occurred within the pixel.

To derive an image endmember set from the satellite data, we made use of the spatial-spectral endmember extraction (SSEE) method described in Rogge et al. (2007, 2012). The number of endmembers extracted by SSEE is defined by the data. SSEE comprises three steps. The image is first divided into equal sized non-overlapping subset regions and a set of eigenvectors that explain the majority of spectral variance is calculated for each subset via singular value decomposition. In the second step the image data are projected onto the local eigenvectors compiled from all subset regions and those pixels that lie at extremes of the vectors are retained as candidate endmembers. The third step averages the candidate pixels with all other pixels within a given spatial window that are also spectrally similar based on a similarity metric, such as spectral angle (Price, 1994). SSEE generally finds several endmembers and many that are similar but spatially independent. Twelve geologically relevant endmembers, shown in Figure 5, were obtained. They display a range of spectral shapes and reflectance amplitudes (bright for felsic and dark for mafic rocks respectively) and in some instances iron absorptions. These endmembers

formed the input of a supervised classification to capture what appeared to be spatially continuous and significant areas. The classification was conducted using the full spectral range available with a color per class. The class color legend is shown in Figure 5.

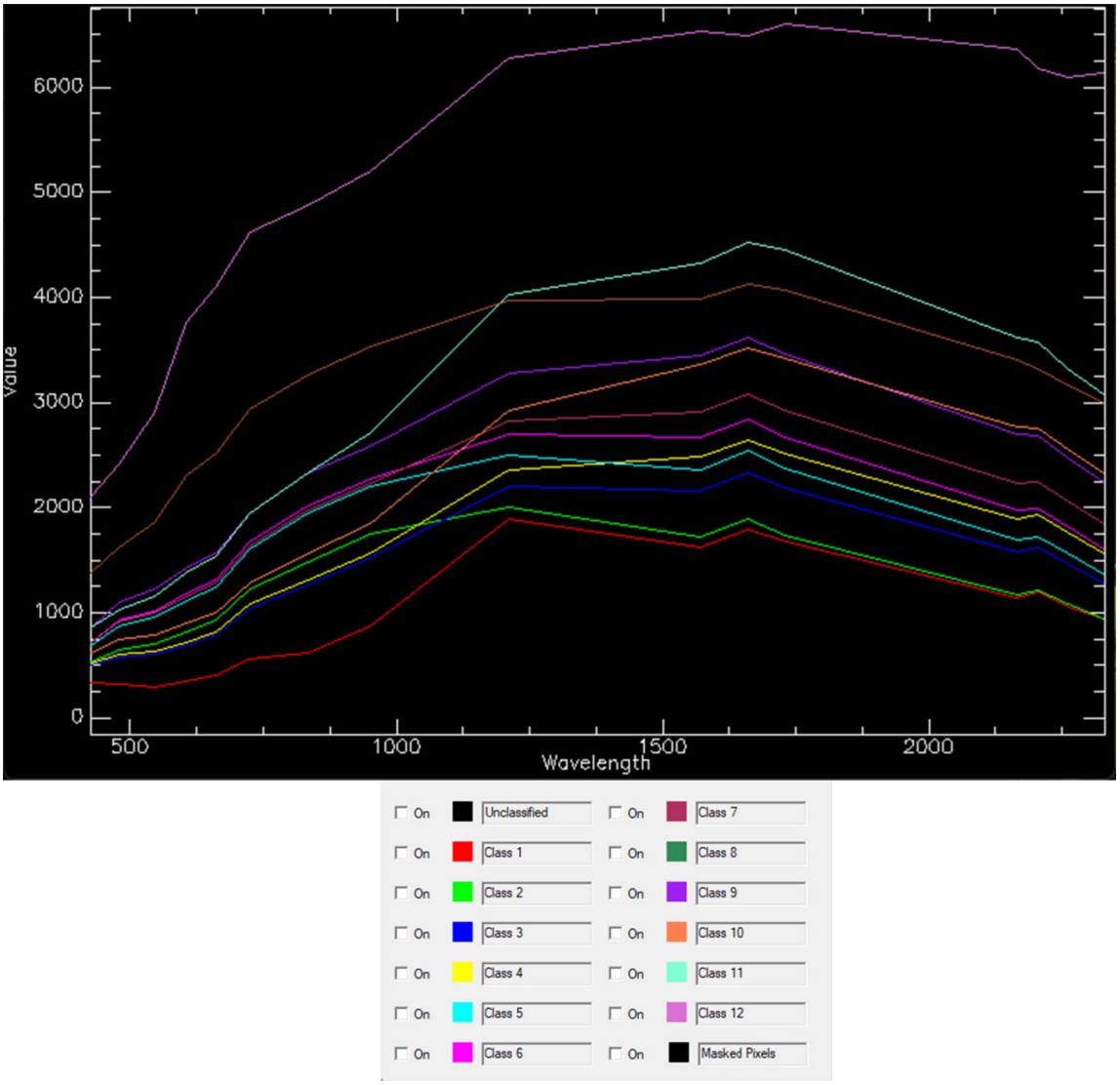

Figure 5. Twelve image endmembers obtained with class color legend for the resulting classification map used in the results section.

3.3.3 Use of Reflectance Spectra Collected in the Field

During fieldwork conducted in the summer of 2023, AER personnel collected reflectance spectra from weathered outcrop surfaces in the Leland Lake and Andrew Lake area using a Terraspec Halo portable spectrometer equipped with a contact probe. As part of this study, ten spectra (Figure 6) that span the spectral variability, encountered in a larger suite of field spectra, were selected for image analysis. These spectra were resampled to the WorldView-3 16 bandpasses prior to their use with the Spectral Angle Mapper (SAM). In contrast to the image spectra shown in Figure 5, the Halo field spectra capture more spectral variability in the shortwave infrared, as seen by pronounced absorptions attributable to white mica (e.g. spectrum 598) and biotite, chlorite (e.g. spectrum 6). These characteristics were exploited with RGB composites of spectral angle maps specifically conducted in the 2165-2300 nm range. These are presented in the results section.

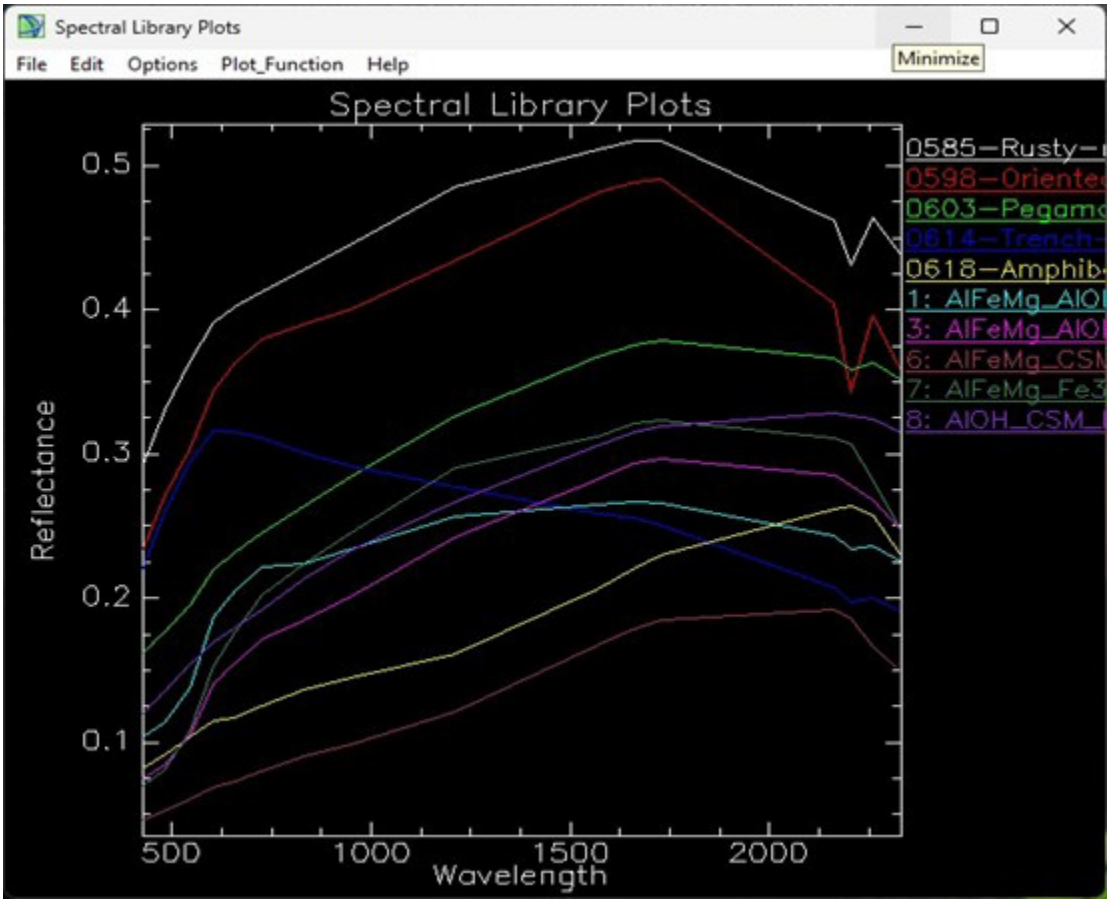

Figure 6. Ten Halo reflectance spectra, resampled to WorldView-3 bandpasses, and selected to capture a range of spectral characteristics and reflectance amplitude. Note several hydroxyl features (>2000 nm) in the shortwave infrared attributable in part to white mica, biotite, and chlorite whose presence and absorption strength influence the shape of the resampled spectra in the last four bands.

4 Results

4.1 Outcrop Map

The outcrop map generated from the WorldView-3 data is shown in Figure 3 and reveals the presence of considerable outcrop in the area. There is an apparent east-west bias in the extent of outcrop revealed by the analysis of the WorldView-3 data which is introduced by the disparity in illumination (extent of shadowing) and vegetation phenology (senescence in the fall scene) between the two available scenes. As also reported in Rivard and Feng (2024) for the same data further north in the Andrew Lake area, the scene captured in June, which occupies the left or western half of the map, revealed more outcrop.

4.2 Geologic Background, Images Used, and Targeted Areas of Investigation

Here we refer extensively to the Godfrey (1980) publication and associated geological maps as we explore potential links between map units and observations from WorldView-3 image products.

The geology covered by the imagery of this study encompasses five maps sheets at a scale of 1:31680. Map sheet 4 (location shown in Figure 2 lower inset) is part of Godfrey and Peikert (1964) whereas map sheets 8,17,18 and 19 are part of Godfrey (1980). The latter four are the focus of this investigation in part due to the more abundant outcrops revealed in the June imagery covering the western portion of the area

and because of what is revealed in imagery. Sixteen main rock types are distinguished on these maps. Most map units depicted on the four map sheets indicate only the predominant rock type, and the minor, smaller-scale lithologic variations are omitted.

As stated in Godfrey (1980) the Precambrian Shield exposed in northeastern Alberta is part of the Churchill Structural Province. The oldest rocks in the Wylie Lake area consist of a migmatitic complex of para- and ortho-gneisses, with minor amphibolite and high-grade metasedimentary rocks; the metasedimentary rocks are currently believed to be Paleoproterozoic, whereas the amphibolite units range from Paleoproterozoic to Archean. This basement complex probably represents multiple cycles of sedimentation, intrusion, deformation, and metamorphism, where ductile or brittle deformation has affected all rock units. The Archean rocks formed under granulite facies conditions and were subsequently overprinted by amphibolite facies conditions during the Taltson orogeny, with only a minor Hudsonian overprint, followed by retrogression shortly afterward. All these rocks were then subjected to a late retrograde greenschist metamorphism.

The study area consists of two main terrains: the mantling granite gneisses, which occupy the Alexander Lake map area (pink unit on map 8, Figure 2 inset) extending along the western margin of the Wylie Lake map area, and the Wylie Lake granitoid complex (brown, orange, yellow units on map 17) which makes up a major part of the Wylie Lake map area. To the south, the complex is overlain unconformably by Athabasca Formation sedimentary rocks, largely obscured by the waters of Lake Athabasca.

Throughout the report we refer to the map units described below whose number are listed on Figure 7 next to the map legend so the reader can link map unit color and label. Here a condensed unit description follows that of Godfrey (1980). The granite gneisses include the biotite granite gneiss (unit 11) and hornblende granite gneiss (unit 12) which incorporate the local occurrence of amphibolite and metasedimentary rocks. Unit 11 (pink on map) is by far the most abundant rock type in map 8 (see Figure 2) and Godfrey (1980) reports up to 13% biotite and 6% chlorite as predominant mafic minerals. Amphibolite (unit 20) is common in the granite gneiss and less so in the Wylie Lake granitoids and exposures are typically 2-25ft in width, many too small to be mapped. It consists of hornblende and feldspar with subordinate quartz, biotite, and epidote. The metasedimentary rocks (unit 31) occur principally within the granite gneisses, but minor patches are also found in the granitoid rocks. The typical lithology is impure quartzite with lesser amount of biotite schist that includes sericite schist, phyllonite and amphibolite. This unit has characteristic orange, brown iron stain weathering. In the Colin Lake area (sheet 4), Godfrey and Peikert (1964) reported that outcrops of metasedimentary and associated rocks occupy about 0.2% of the total outcrops in the area. The granitoid rocks dominate the Wylie Lake map area (sheet 17) and include seven map units (123,124,126,131,133,134,135). Godfrey (1980) reports up to 26% biotite and 9% hornblende in these rocks from the analysis of 7 samples.

As part of the results, we present a suite of image products described in the methods, first for the total area covered by imagery, to set the context of synoptic observations, and then for specific subsets of interest. An inherent challenge in the interpretation of such products is the environment that was imaged, which is partially forested and can lead to false image interpretations despite best efforts to remove the influence of vegetation in imagery. In addition, as indicated in section 4.1, imagery obtained at different times of the year offer different potential for capturing outcrops. In this case there are clearly poorer results in terms of outcrop recovery in the October scene covering the eastern parts of the map area which impacts lithological inferences.

Another inherent challenge is the nature of the geology of the area that has a predominance of felsic rocks that may display limited spectral diversity (e.g., similar mineralogy). Also, varying schists and amphibolites that can harbor hydroxyl-bearing minerals (e.g. white mica, biotite, chlorite, amphiboles), of known remote sensing detection potential, are challenging to convey on maps, as stated by Godfrey (1980), as they occur at a variety of scales and are of varying continuity. This can limit inferences between image domains and a map that may not always convey their occurrence and this despite a map scale of 1:31680. Our approach for this report is to establish potential correlations between map units and

image domains, assign potential lithologic labels to image observations with the recognition that such observations will need field validation.

Shown in Figure 7 is the White Mica index because it highlights several regions (five numbered white polygons) with variability in index values. It is juxtaposed to the portions of the five geologic map sheets that encompass the WorldView-3 imagery along with the map legend and map unit #. The White Mica index image is repeated in Figure 8 and juxtaposed to the Rock Fe and Rock MF images. In all instances the index values are displayed using a rainbow color table shown in Figure 8 with red allocated to highest values. Figure 8 can be examined in conjunction with Figure 9 which displays two RGB composites of spectral angle maps (SAM) derived from Halo endmembers (EM) (spectra on Figure 6) while applying SAM to the 2165-2300 nm spectral range. Subsequent figures (Figure 10-Figure 16) provide image enlargements of the five areas and related portions of the geologic map.

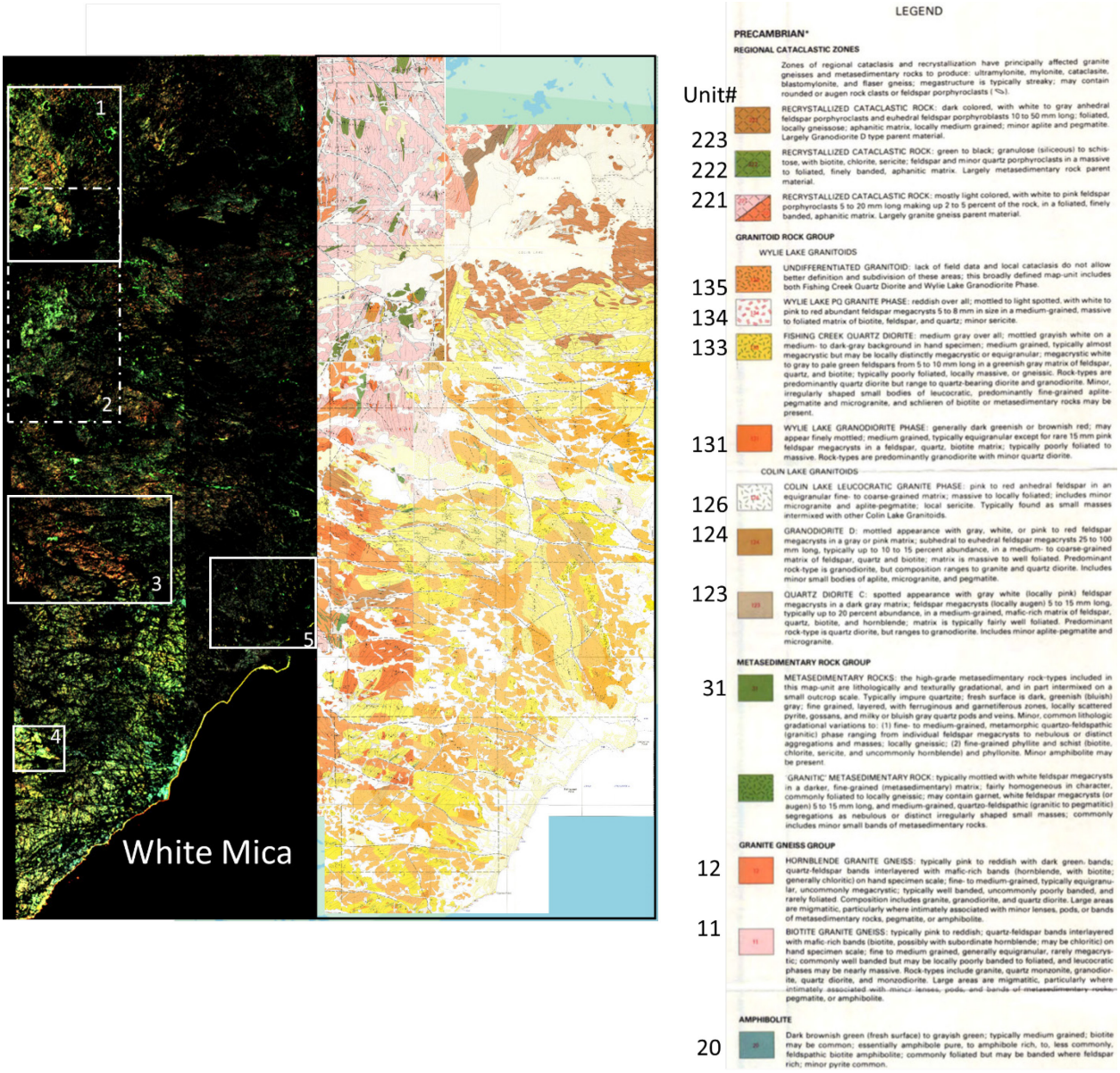

Figure 7. Geologic map (centre) along with legend (right) taken from Godfrey (1980) and the White mica index image (left). Five numbered areas highlighted by a white polygon are enlarged in subsequent figures.

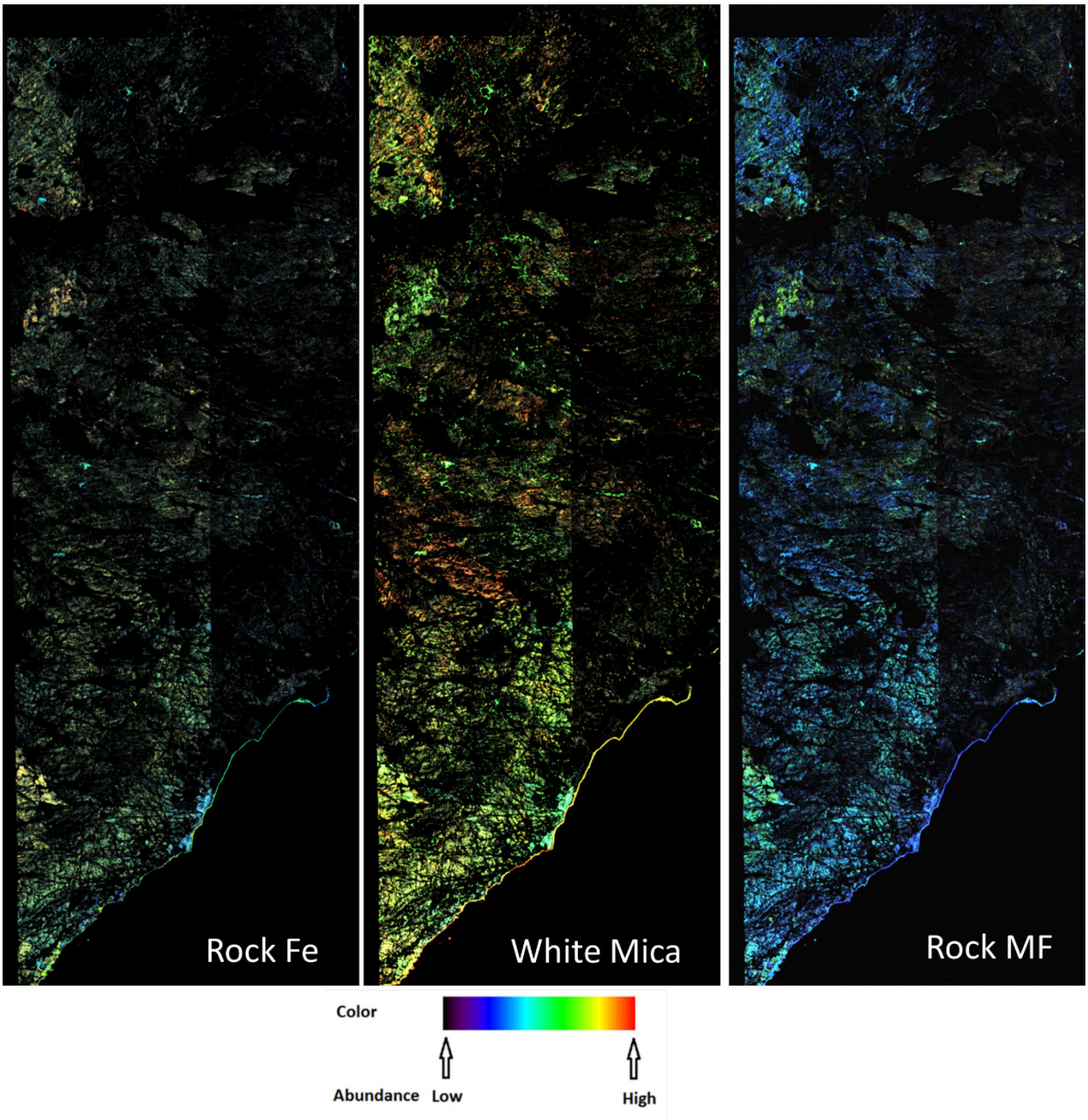

Figure 8. Key index images with white labels in lower right corner. Refer to equations 4, 5, and 6 for computation of indices.

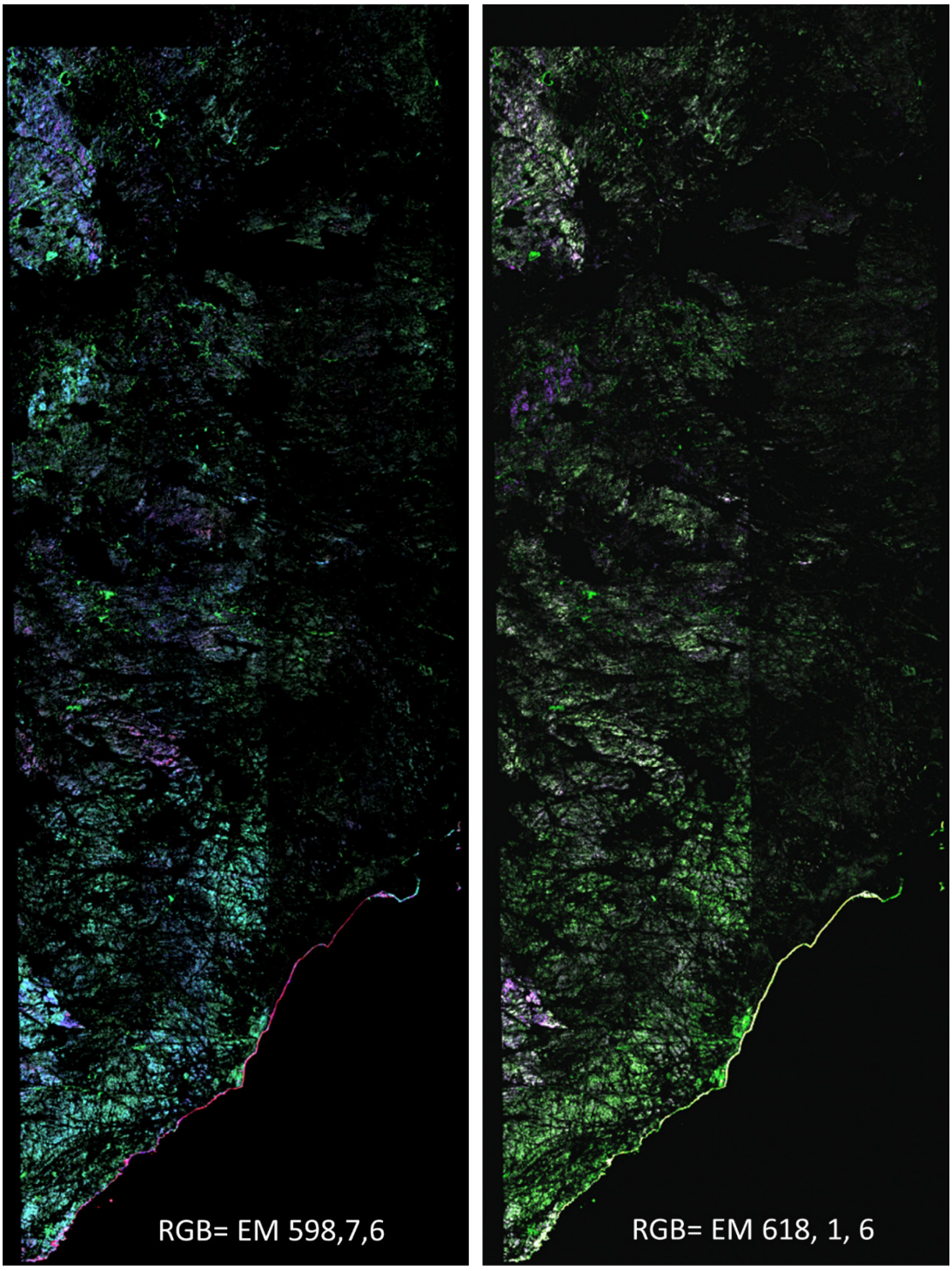

Figure 9. RGB composites of spectral angle maps (SAM) derived from Halo endmembers (EM) shown on Figure 6. SAM was applied to the 2165-2300 nm spectral range.

4.3 Areas of Investigation

4.3.1 Observations for Area 1

Area 1 shown on Figure 7 captures an area of approximately 6 by 2 km occupied by several outcrops of moderately elevated White Mica index values (red to orange). The entire area is predominantly mapped as biotite granite gneiss (pink unit 11) with subordinate hornblende granite gneiss (orange unit 12) and metasedimentary rocks (green unit 31). Figure 10 provides a closeup and includes a RGB composite of spectral angle maps derived from Halo endmembers (spectra on Figure 6) as well as a classification map of image endmembers (all spectra on Figure 5). The classification map is dominated by two domain types (orange and magenta) that follow the fabric (e.g. regional foliation on map). Three of the broader continuous domains of the orange class are highlighted in dotted polygons (Figure 10) and we cannot suggest any direct correlations to map lithologic patterns. Note that the image endmember classification is conducted on the full spectral range and would be driven by broad differences in the spectral shape amongst endmembers including the presence of iron oxide features resulting from surface weathering (or gossans). It is feasible that it captures lithological variability within the biotite granite gneiss map unit.

Two polygons on the White Mica Index image highlight some of the highest values seen here and these domains do not track the patterns seen on the image endmember classification map that has low sensitivity to the presence of white mica. Again, the White Mica image may reflect further variability with this gneissic unit. Lastly the EM598,7,6 RGB, designed using Halo field spectra to contrast mafic rocks (e.g. EM6) with felsic rocks that incorporate absorptions due to white mica, biotite and chlorite (e.g. EM 598 and 7), highlights its own regional pattern. It may result from the influence of varying abundance of metasediments that contain mafic minerals. Further along these lines, RGB EM 618,1,6 (Figure 11) also derived from field spectra, uniquely highlights a suite of white pixels which fall near or within mapped metasediment (green unit 31).

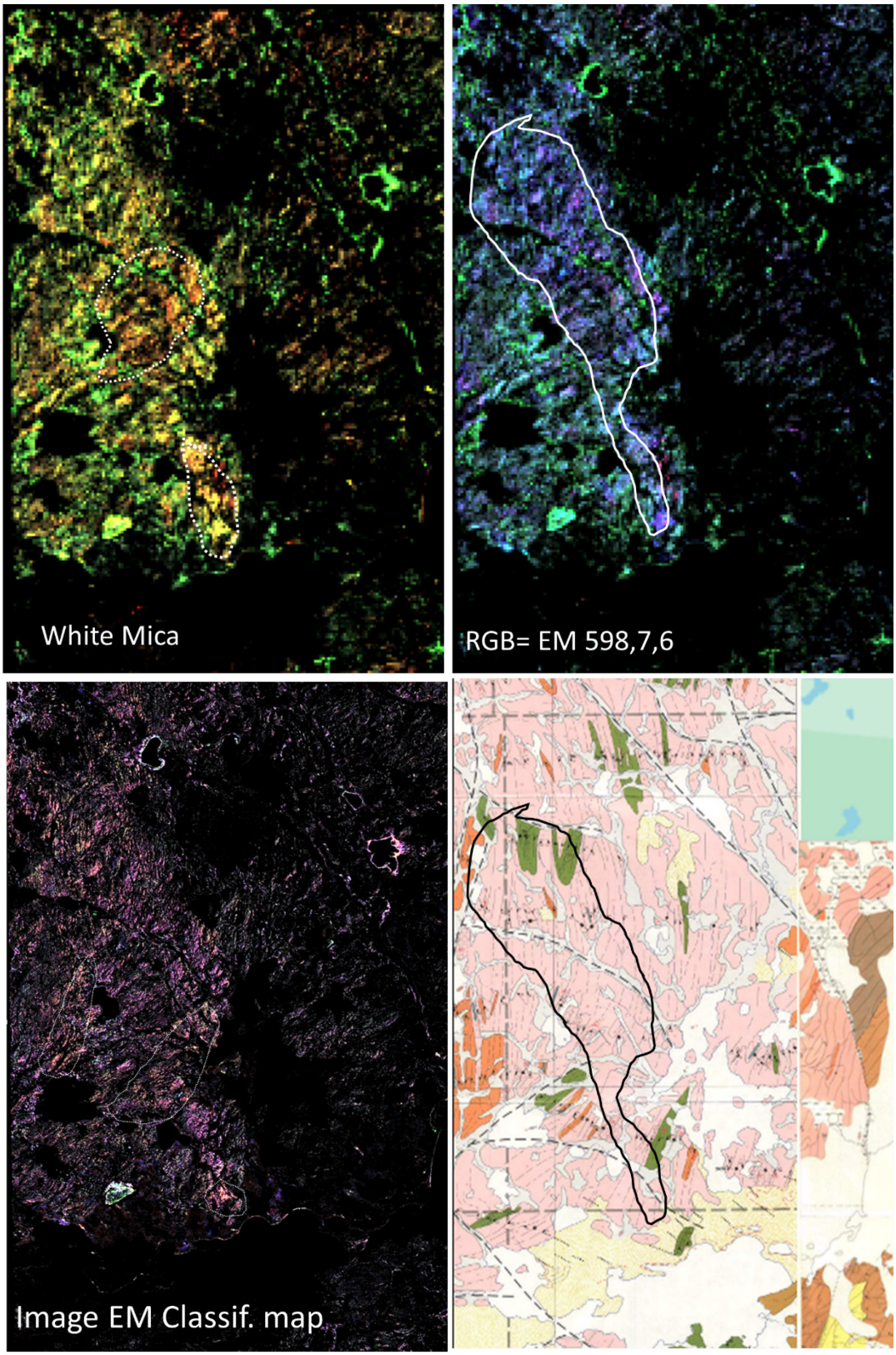

Figure 10. Enlargement 1 on Figure 7. The area presents distinctly high (red) White Mica index values and appears blue (EM6) on RGB 598, 7, 6. Further detail shown on Figure 11.

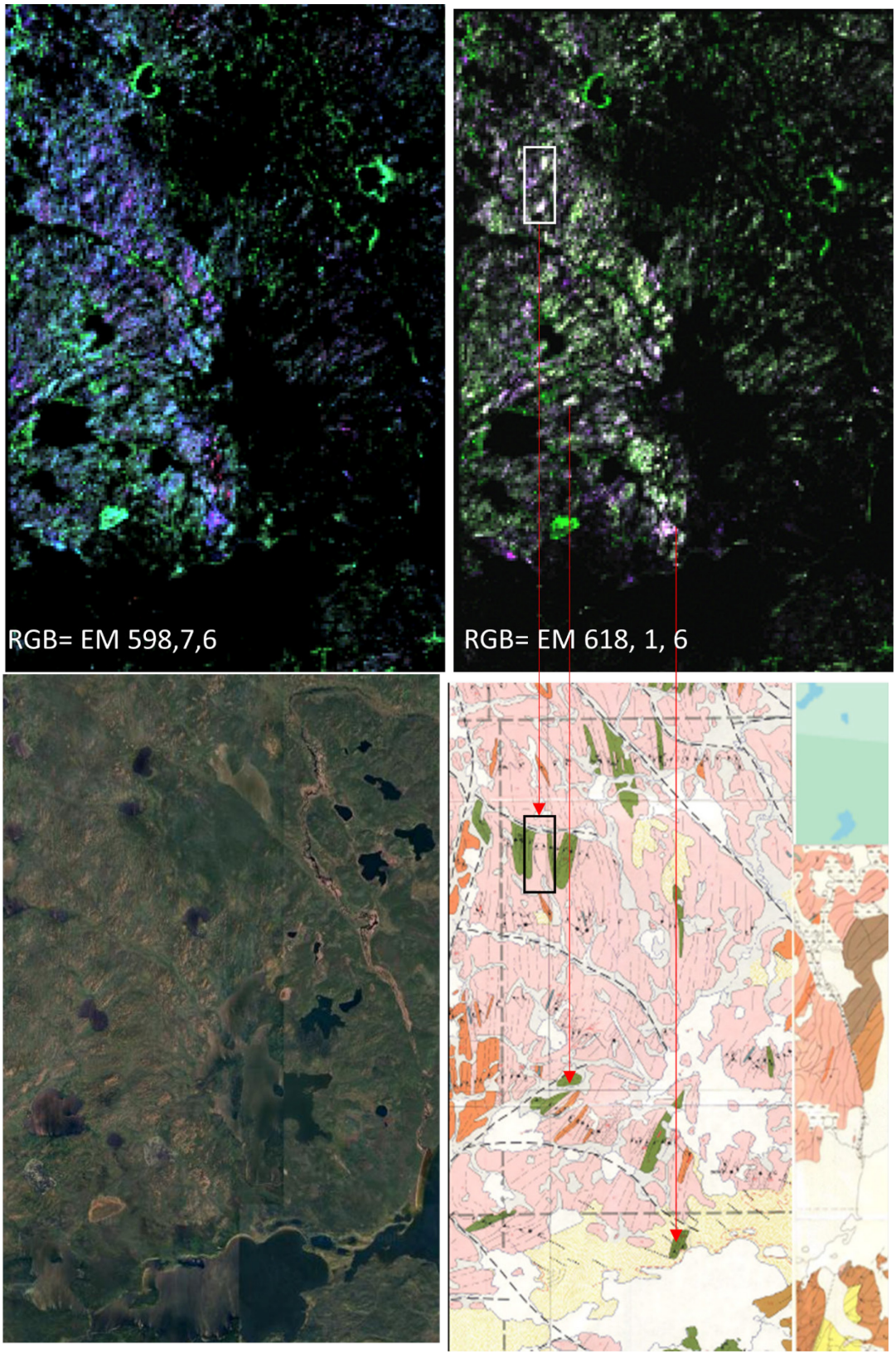

Figure 11. Enlargement 1 on Figure 7. The RGB 618,1,6 displays white domains that may correspond to map unit 31 labeled as metasedimentary rocks.

4.3.2 Observations for Area 2

Area 2 on Figure 7 captures an oval image region that stands out on all index images (Figure 8) and RGB composites of spectral angle maps derived from Halo endmembers (Figure 9). It is noteworthy primarily because it presents rather uniform image characteristics on all these images suggesting it represent a particular lithotype. It does not, for example, present high White Mica index values that could point to localized alteration. Upon closer look via Figure 12, one sees that the region highlighted in imagery falls between geologic map sheets 8 and 17 but is largely encompassed by two map units: northern parts in the Fishing Creek quartz diorite (olive unit 133) and in the south undifferentiated granitoids (orange unit 136). The undifferentiated granitoids are said to be primarily composed of Fishing Creek quartz diorite and Wylie Lake granodiorite. It is therefore reasonable to assume that the imagery highlights the Fishing Creek quartz diorite in this part of the study area.

According to Godfrey (1980) the Fishing Creek quartz diorite is light- to medium-gray overall in outcrop and the rock is commonly poorly foliated, but is locally gneissic or massive. The modal mineralogy of six samples shows biotite content up to 20% with an average of 10%. The primary regional unit surrounding the Fishing Creek quartz diorite in this map area is biotite granite gneiss (pink unit 11). Biotite granite gneisses are typically composed of quartz-feldspar felsic layers alternating with biotite-rich (occasionally with minor hornblende), mafic layers. Chloritization of biotite is very common. The modal mineralogy of nine samples shows biotite content up to 12% and averaging 6%, and a chlorite content up to 6% averaging 1.3%. This limited sample analysis suggests a similar mafic mineral content for both rock units but the blue tones of the biotite granite gneisses on the Rock MF imagery (Figure 12), that was designed to contrast mafic and felsic rocks, suggests that overall it has a distinctly lower mafic content than the Fishing Creek quartz diorite.

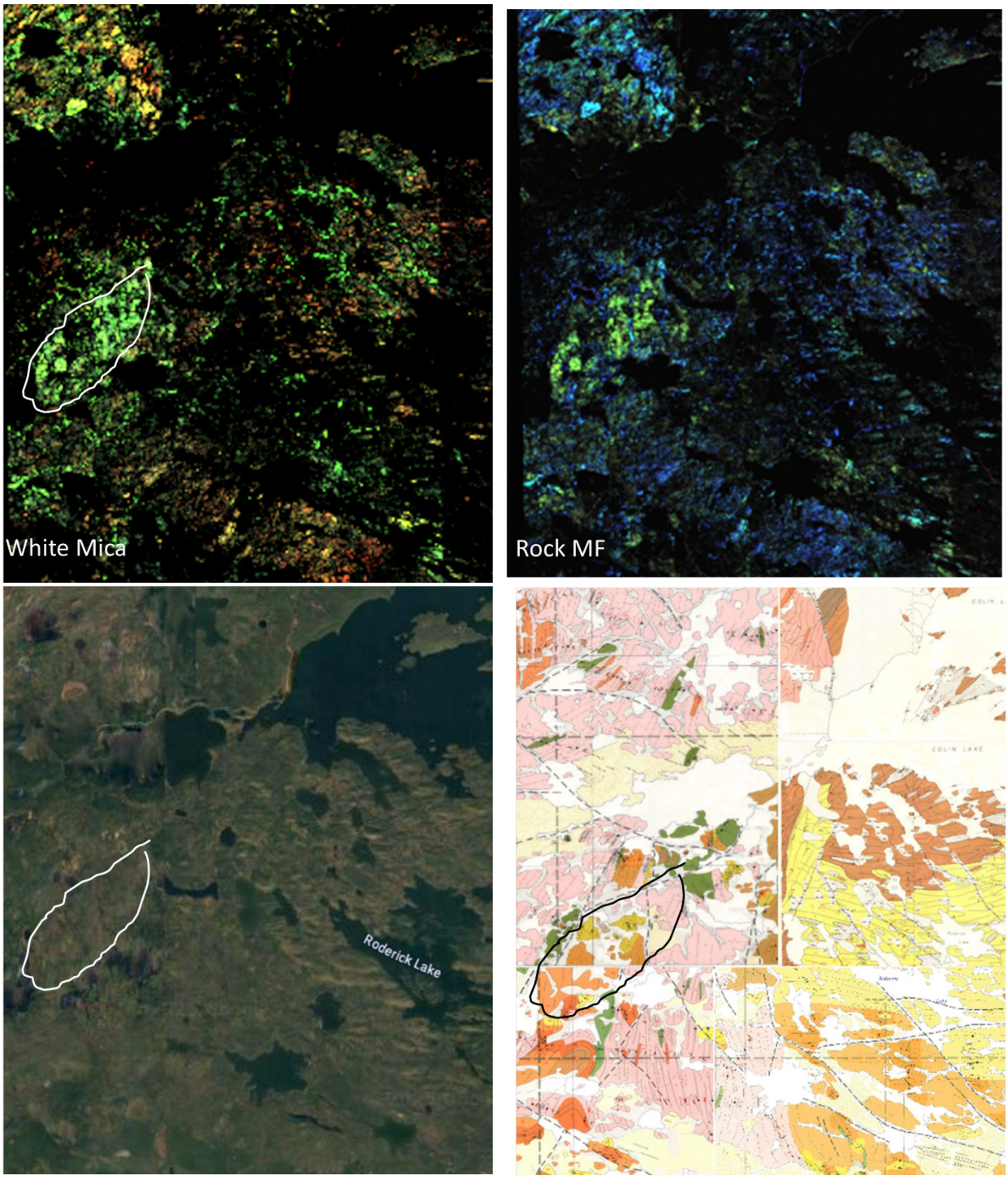

Figure 12. Enlargement 2 on Figure 7. The area presents distinctly mid (green) White Mica index and Rock MF values.

4.3.3 Observations for Area 3

Area 3 was selected because it captures a region of elevated White Mica index values (Figure 7 and Figure 13), the most prominent highlighted by an oval polygon on Figure 13 and a square polygon to the west. The whole of area 3 encompasses five mingling felsic units (Figure 13: units 131,132,133,136,137)

namely the Wylie Lake granodiorite (unit 131), the Wylie Lake granodiorite E (unit 132), the Fishing Creek quartz diorite (unit 133), undifferentiated granitoids (unit 136), and the Wylie Lake granodiorite D (unit 137). Both polygons mentioned above encompass 5 of these 6 felsic units which also occur elsewhere in the area and on that basis, we suggest that the elevated White Mica index values are unrelated to any given map unit and may represent a local alteration though we cannot offer an explanatory mechanism.

Also shown on Figure 13 are the two RGB composites of spectral angle maps derived from Halo endmembers (EM) seen on Figure 6. The EM 598,7,6 RGB, designed to contrast mafic rocks (e.g. EM6) with felsic rocks that may incorporate absorptions due to WM, biotite and chlorite (e.g. EM 598 and 7), highlights substantial portions of the polygons described above. But within the upper right corner polygon and within the SE tip of the oval polygon, RGB EM 618,1,6 uniquely highlights a suite of white pixels which, in the case of the first polygon, fall within a mapped metasediment map unit (green unit 31). Note that these white pixels are also highlighted in the image EM classification map (Figure 13, orange areas shown by white arrows). It may be that a combination of RGB's is well suited to highlight metasediments in these gneisses which are not abundantly mapped in this map sheet. Godfrey (1980) indicated that their range in size and continuity presents a challenge for their representation in maps.

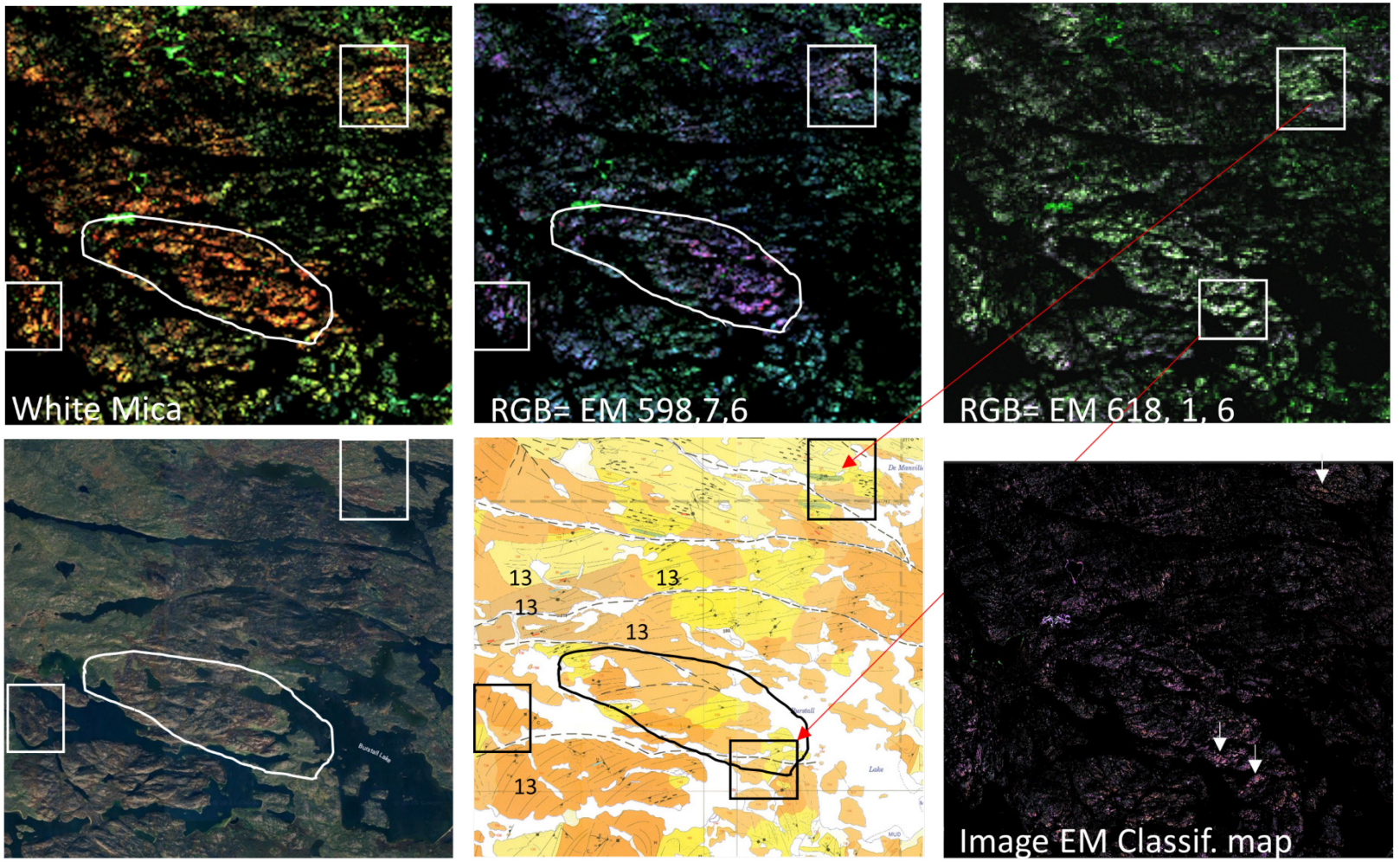

Figure 13. Enlargement 3 on Figure 7. The area presents distinctly high (red) White Mica index values and appears blue (EM6) on RGB 598, 7, 6. The RGB 618,1,6 displays white domains corresponding to orange areas (white arrows) in the image EM classification map.

4.3.4 Observations for Area 4

Area 4 (Figure 7) was selected because it is prominent on all three index images (White Mica, Rock Fe and MF, Figure 8) and both RGB of Halo endmembers (Figure 9). It encompasses two image domains here illustrated with the White Mica index that highlights three highs (red pixels) shown on Figure 14 with the white arrows while immediate surrounding areas appear magenta on the RGB EM 618-1-6. Comparison to the geological map does not reveal a direct correlation to map patterns, the region being occupied by felsic rocks, namely the Fishing Creek quartz diorite (yellow, unit 133) and Wylie Lake granodiorite (brown unit 131).

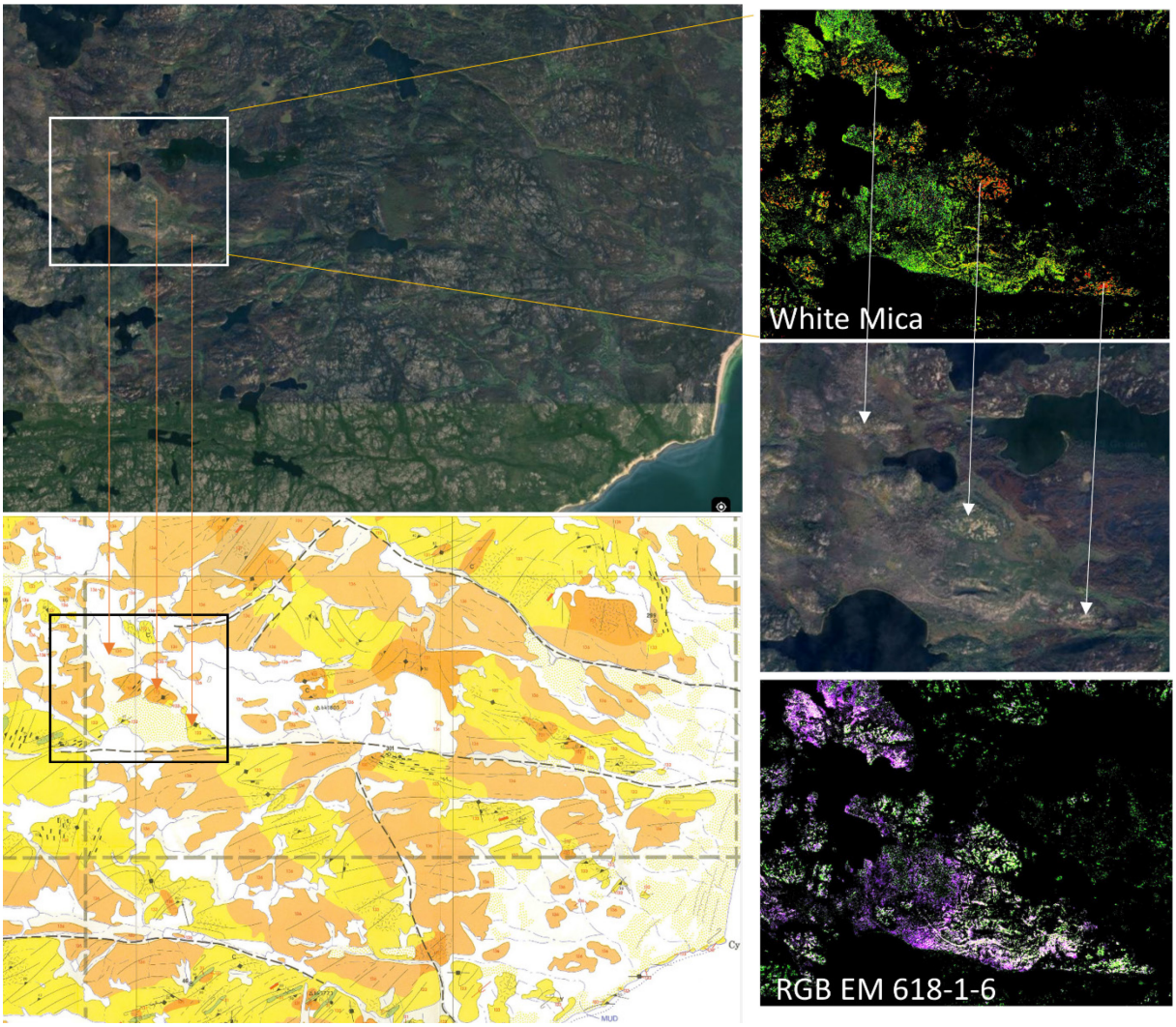

Figure 14. Enlargement 4 on Figure 7. The area presents distinctly high (red) White Mica index values that fall within map unit 131 (brown) and 133 (yellow).

4.3.5 Observations for Area 5 with Reported Mineral Occurrences

Here we report observations for area 5 on Figure 7, an area with mineral occurrences reported in the past. Godfrey (1980) devotes a section in his report to mineral occurrences and the uranium potential of the basement gneisses and granitoids and the Athabasca Formation. He reports widespread radioactivity, associated with abundant yellow stains on the outcrop in an area near Winnifred Lake within map 18 (southeast portion of our study). He states that for the most part, this radioactivity is associated with leucocratic segregations in Fishing Creek quartz diorite (map unit 133); some radioactivity is also

associated with granitic metasediments and Wylie Lake granodiorite (unit 131). He then states that at the time of the report attention has focused on the uranium potential of the Athabasca Formation and the sub-Athabasca basement regolith. He also reports concentrations of angular Athabasca sandstone rubble along the Lake Athabasca shoreline near Greywillow Point and towards Falling Sand Point as a possible indication that the area is underlain by the Athabasca Formation (map 18).

Godfrey states that the Athabasca Formation in Saskatchewan is known to be underlain by highly altered, regolithic basement material and that such material is exposed in a shoreline section about 1.1 m thick just north of Greywillow Point. Highly altered, intensely hematite-stained basement rocks that show no sign of having been water-transported are cut by numerous fractures and quartz veinlets. He reports that cross-cutting quartz veinlets in the basement regolith north of Greywillow Point suggests its proximity to a fault zone. The extension of shears mapped in nearby basement rocks (map 18) would intersect overlying Athabasca Formation rocks to the south and east, beneath the waters of the present Lake Athabasca. He concludes that these observations provide a possible incentive in the exploration for uranium deposits within and close to the Athabasca Formation in this part of Alberta.

Here we report three locations that may relate to the geological context elaborated by Godfrey near Greywillow point seen in Figure 15. Figure 15 display the mineral occurrences map obtained from AER, which consist primarily of uranium occurrences near Lake Athabasca but also inland. Adjacent to this map we show elevated White Mica index values at two locations (white arrows) which are also seen in a Halo endmember SAM RGB. Figure 16 enables more detailed observations where three areas encompassing outcrops of elevated White Mica index values are observed (see white arrows). These areas span 10’s to 100’s of meters and from west to east respectively fall within the Wylie Lake granitoid E (pale yellow unit 132), the Fishing Creek quartz diorite (dark yellow unit 133), and undifferentiated granitoid (pale brown unit 136) (red arrows, Figure 16). Note that none of these locations relate to locations shown on the mineral occurrence map on Figure 15. However, they do define a linear ESE trend and may mark alteration associated with a late ESE fault. The white polygon on Figure 16 marks a region encompassing three trends of outcrops with anomalous values, but the absence of map coverage precludes a link to prior geological mapping.

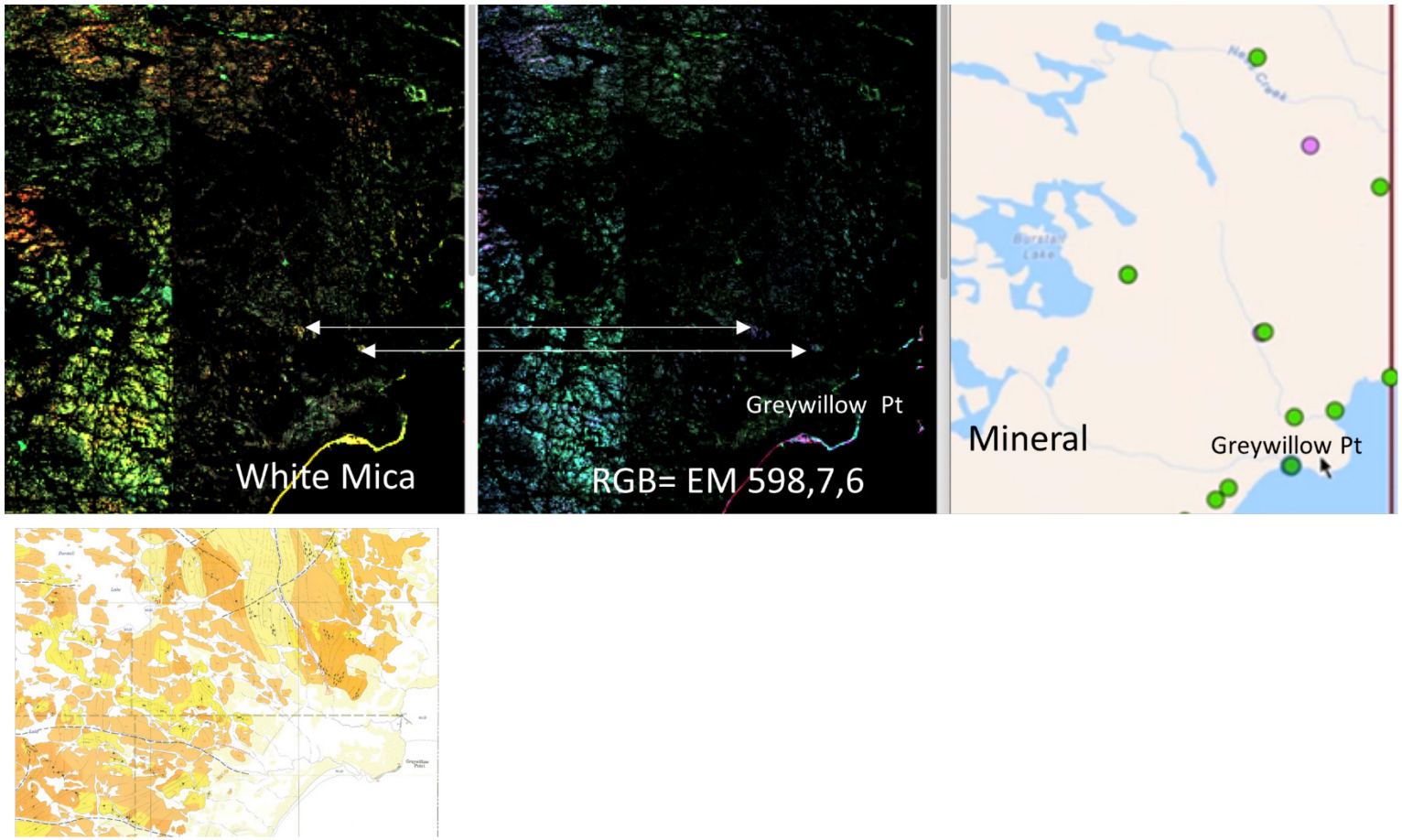

Figure 15. Enlargement 5 on Figure 7. The area presents distinctly high (red) White Mica index values also discernable on RGB 598, 7, 6. More detailed views are on Figure 16.

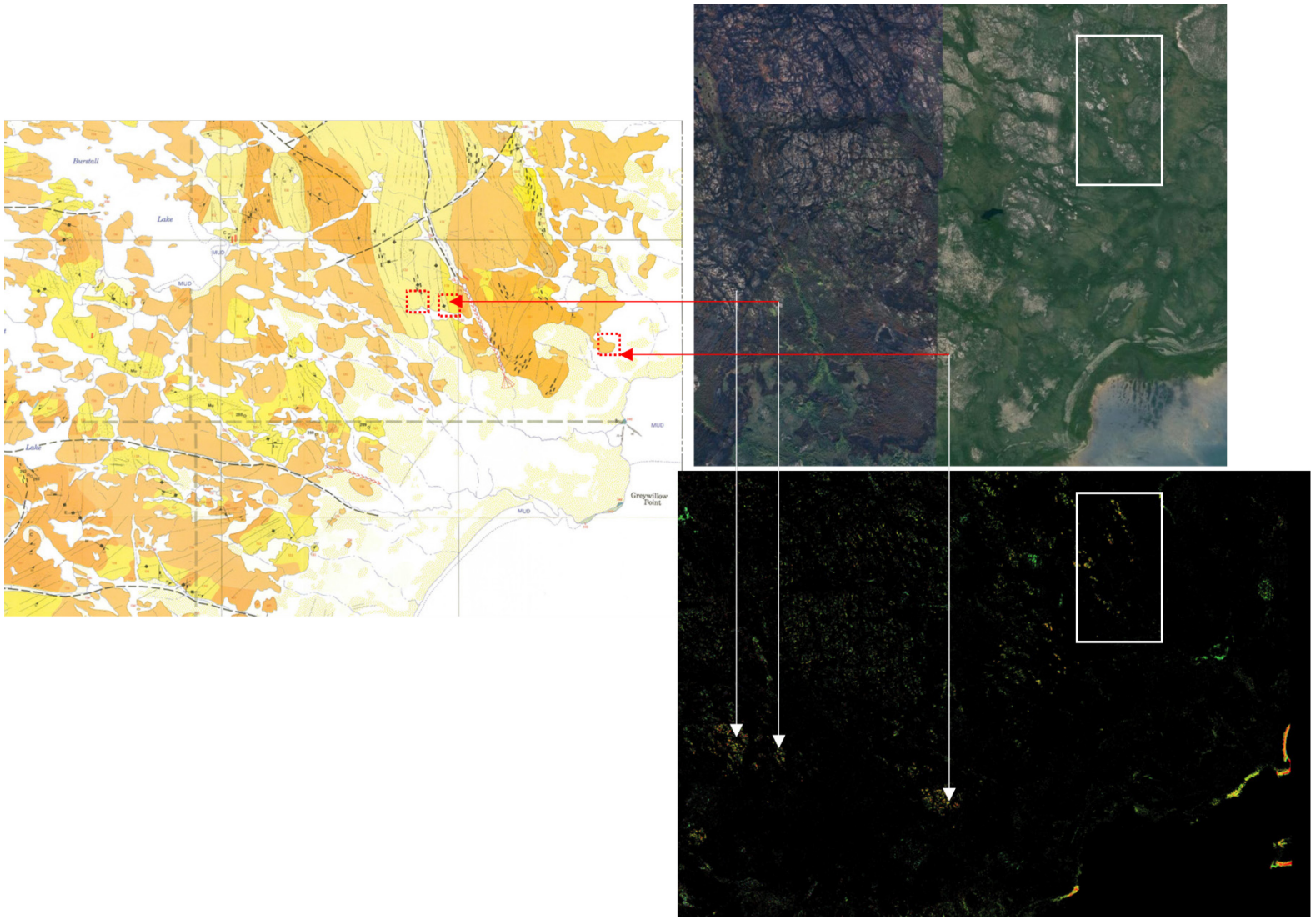

Figure 16. Enlargement 5 on Figure 7. Four areas (red dashed polygons and white polygon) present distinctly high (red) White Mica index values that fall within the Wylie Lake granitoid E (pale yellow unit 132), the Fishing Creek quartz diorite (dark yellow unit 133), and undifferentiated granitoid (pale brown unit 136). Dashed black marks on the map, neighboring the areas of interest, define fault zones. The white polygon lies outside of map 18.

5 Discussion and Conclusion

5.1 Image Acquisition

This study made use of the southern extension of the two images utilized in the 2024 study for Andrew Lake (AER/AGS Special Report 123). As reported in that study, the October 2021 scene, covering the eastern portion of the imaged area, enabled the capture of outcrops to a much lower extent than the June 2022 scene and likely due to the lower solar illumination and the presence of leaf litter on outcrop.

5.2 Lithological Inferences

This study encompassed five different map sheets and a greater diversity and spatial variability of felsic rock units than encountered in the Leland Lake (Rivard 2023) and Andrew Lake studies (Rivard and Feng 2024). This diversity and variability meant that it was often difficult, or not possible, to relate image and map patterns. Despite this challenge the report highlights four regions (Areas 1-4, Figure 7) where relatively large unique image domains are seen. In the opinion of the authors these likely result from regional mineralogical variability within gneissic units or variability in abundance of metasedimentary rocks and/or amphibolite within the gneisses, variability that could be portrayed on maps at a scale of 31680. In contrast, the fifth area (Area 5, Figure 7) does not highlight large image domains but three 100-200m areas with elevated white mica index values defining a linear ESE trend. It is feasible that these mark alteration associated with a late near ESE fault and be of relevance to uranium exploration. This portion of the study area should be the subject of more scrutiny.

6 References

Godfrey, J.D., and Peikert, E.W. 1964. Geology of the Colin Lake district, Alberta. Research council of Alberta preliminary report 62-2. 26 pages.

Godfrey, J.D. 1980. Geology of the Alexander-Wylie lakes district, Alberta. Alberta Research Council Earth Sciences Report 78-1. 24 pages.

Langenberg, C.W. and Eccles, D.R. 1996. Metallic mineral occurrences of the exposed Precambrian shield in northeastern Alberta; Alberta Energy and Utilities Board, EUB/AGS Bulletin 64, 71 p.

Mars, J.C. 2018. Mineral and lithologic mapping capability of WorldView 3 data at Mountain Pass, California, using true- and false-color composite images, band ratios, and logical operator algorithms. Economic Geology, v. 113, no. 7, 1587–1601

Price, J. C. 1994. How unique are spectral signatures? Remote Sensing of Environment, 49, 181–186.

Rivard, B. 2023. Analysis of WorldView-3 satellite imagery for the Leland Lakes area, Alberta. AER/AGS Special Report 116, 20 pages.

Rivard, B. and Feng J. 2024. Analysis of WorldView-3 satellite imagery for the Andrew Lake area, Northeastern Alberta. AER/AGS Special Report 123, 19 pages.

Rogge, D., Bachmann, M., Rivard, B., and Feng, J. 2012. Spatial sub-sampling using local endmembers for adapting OSP and SSEE for large-scale hyperspectral surveys. IEEE Journal of Selected Topics in Applied Earth Observations and Remote Sensing, 5, 183–195.

Rogge, D., Rivard, B., Zhang, J., Harris, J., Feng, J., and Sanchez, A. 2007. Integration of spatial-spectral information for the improved extraction of endmembers. Rem. Sens. Environ. 110(3), 287-303.

Shedlovska, Y.I., and Hnatushenko, V.V. 2019. Shadow Removal Algorithm for Remote Sensing Imagery. IEEE 39th International Conference on Electronics and Nanotechnology (ELNANO), pp. 818-822. DOI:10.1109/ELNANO.2019.8783642report delivered

7 Appendix 1: List of Digital Deliverables

Georeferenced mosaic data for the following products are provided in ENVI format and in Geotiff format for visually enhanced products.

Product	File name or folder	Number of files
1) SAM classification map for 2160-2330 nm	2160-2330-SAM class	1 (envi, img)
2) SAM RGB of endmembers 598, 7, and 6 for 2160-2330 nm	2160-2330-SAM-RGB-EM598_7_6	1 (envi, geotiff)
3) SAM classification map for all VNIR-SWIR bands	Full-SAM-class	1 (envi, img)
4) Spectral library of image endmembers	Image Endmembers-lib	1 (envi, lib)
5) Classification map of image endmembers	ISO10-13-3	1 (envi, img)
6) Halo spectral library	Merged-2023-2024	1 (envi, lib)
7) Halo spectral library resampled to WorldView-3 bands	Merged-2023-2024-WV3	1 (envi, lib)
8) SAM RGB of endmembers 618, 1, and 6	SAM-RGB-EM618_1_6	1 (envi, geotiff)
9) White Mica index	WylieLake-OH	1 (envi, geotiff)
10) RGB of Rock Fe, White Mica, and MF indices	WylieLake-RGB-Fe-Oh-MF	1 (envi, geotiff)
11) Rock Fe index	WylieLake-Rock-FeMg	1 (envi, geotiff)
12) Rock MF index	WylieLake-Rock-MF	1 (envi, geotiff)
13) Rock White Mica, Chlorite, and Biotite index	WylieLake-WM-Chl-Bio	1 (envi, geotiff)